



OPEN

Particle breakage characteristics of calcareous sand under confined compression tests

Zhijiang Li^{1,3}, Biwen Zhang²✉, Yani Lu^{1,3}✉, Xinlian Chen^{1,3}, Yan Wu⁴, Mingxing Luo^{1,3} & Li Zhong^{1,3}✉

Calcareous sand is a widely used foundation material in marine engineering. Particle breakage can lead to an increase in its compressibility, affecting the safety and stability of structures. The compression characteristics and particle breakage effects of calcareous sand were analyzed through 33 sets of confined compression tests using calcareous sand specimens. The initial void ratios of the specimens were set between 1.0 and 1.3, and three gradations were selected: 1–2 mm, 0.5–1 mm and 0.25–0.5 mm. Moreover, the loading–unloading–reloading tests were conducted. The initial test was loaded to a maximum of 2 MPa and began to unload to 0.4 MPa and then to load to 6 MPa. The test results indicated that the deformation of calcareous sand during compression was mainly plastic deformation, which was irreversible or irrecoverable. With the increase in the vertical pressure, the compression curves of the specimens under different initial void ratios gradually converged to a common straight line. With the increase in the loading, the existence of particle size less than 0.074 mm in the specimen showed a decreasing trend, and all types of particle breakage indices showed an increasing trend. The particle size of the specimen was larger, the value of the breakage index was larger. Comparison of multiple breakage indices proposed by researchers revealed that the breakage indices increased with the increase in the vertical pressure. Some breakage indices cannot adequately represent the wholeness of the gradation curves and are not easy to be used as breakage index. Generally, the relative breakage index of Hardin B_r was smaller than the relative breakage index of Einav B_{e_r} , and there was a close relationship between the two. The test results can provide theoretical guidance for the construction of calcareous sand islands and reefs.

Keywords Confined compression, Calcareous sand, Particle breakage, Relative breakage index

With the development of marine economy, the gradual improvement of human marine resources development capacity and the gradual enhancement of marine ecological environmental protection awareness, as well as the need for comprehensive marine management, which makes the number and scale of modern marine engineering increasing. The coral island and reef filling is generally on a vast area of shoal around the reef plate. A large amount of marine sand inside the lagoon is dredged out by a dredger, the sand–water mixture is discharged through the pipeline to the shoal for filling, the water in the sand is drained to a certain elevation, and then the building foundation is formed through the pre-pressure and other foundation treatment methods. Therefore, most of the islands and reefs sediments in these marine engineering are dominated by calcareous sand. Calcareous sand is a specialized medium composed primarily of calcium carbonate and other insoluble carbonates, and an important characteristic of such materials is the particle breakage effect. The particle breakage effect leads to the variation in the gradation structure, void ratio and particle shape of calcareous sand, significantly affecting the compression characteristics of calcareous sand^{1–4}. The complex properties of the marine environment and the unique properties of calcareous sand present significant challenges in ensuring the stability of engineering structures. Therefore, the study of the effects of particle breakage characteristics on compression characteristics of calcareous sand has important theoretical significance and application value.

In response to the description of particle breakage, researchers have long proposed various quantitative indicators of particle breakage. For example, Miura and O-Hara⁵ performed the triaxial shear test of coarse

¹School of Civil Engineering, Hubei Engineering University, Xiaogan 432000, Hubei, China. ²School of Civil Engineering and Architecture, Wuhan University of Technology, Wuhan 430070, Hubei, China. ³Hubei Small Town Development Research Center, Hubei Engineering University, Xiaogan 432000, Hubei, China. ⁴Department of Urban Construction, College of Technology, Hubei Engineering University, Xiaogan 432000, Hubei, China. ✉email: zhangbiwen@whut.edu.cn; lyn2016@hbeu.edu.cn; zhongl@hbeu.edu.cn

granular material, and proposed to quantify particle breakage in terms of the incremental particle surface area B of the specimen. Marsal⁶ proposed to characterize the amount of particle breakage by taking the maximum value B_M of the particle size content difference between the two particle gradation curves on the sieving curves obtained before and after the tests in the study of granular material for the Mica dam. Lee and Seed⁷ conducted experimental research on the earth and rock dam backfill material, and proposed to use the ratio of the particle size with a mass percentage of 15% on the sievingcurve obtained before and after the tests to express the degree of particle breakage B_{15} . Lade et al.⁸ used the difference in the ratio of effective particle size d_{10} before and after particle breakage as the particle breakage metric B_{10} in the study of the relationship between the particle breakage and permeability. Some researchers selected a particle size d_{60} with a mass accumulation percentage of 60% as the characteristic particle size, and the difference between this characteristic size before and after compression was used to define the particle breakage index $B_{60}@@@^9$.

To overcome the shortcomings of previous particle breakage metrics that only considers a single particle size, Hardin¹⁰ proposed the concept of relative breakage index to evaluate the degree of particle breakage. That is, the area A enclosed by the gradation curve of sandy soil and the 0.075 mm particle size cutoff line is defined as the breakage potential, and the difference between the breakage potential before and after the tests is defined as the total breakage, then the relative breakage index B_r is the ratio of the total breakage to the breakage potential before the test. Einav¹¹ eliminated the limitation of the maximum particle size line of 0.074 mm on the basis of relative breakage index of Hardin¹⁰, and introduced the concept of ultimate particle gradation curve, and modified the breakage potential and total breakage, and proposed the particle breakage metric B_e . Meanwhile, different scholars have proposed different methods to quantify particle breakage^{12,13}. Generally, area and volume calculations are easier for particles with regular shapes, but the shape of particles in practical engineering is complicated, so it is impossible to calculate the area and volume of particles. The mass measurement is relatively convenient, but some breakage indices have some restrictions on the use, which need to be further investigated. At present, the three breakage indices proposed by Marsal⁶, Hardin¹⁰ and Einav¹¹ are widely used.

The most commonly used test in soil mechanics to determine the compression deformation characteristics of soil is confined compression test¹⁴⁻¹⁷. Lateral confinement is where the lateral displacement is imposed by the test apparatus during the compression process resulting in no lateral deformation during the test, and the specimen can only be vertically deformed when subjected to vertical loading¹⁸⁻²⁰. Confined compression tests have also been widely used for mechanical characterization of calcareous sand²¹⁻²⁶. For example, Pestana and Whittle²⁷ discovered that the compression characteristics of calcareous sand are related to the initial relative density through the confined compression test, and established a simple four-parameter elastic-plastic model to describe the one-dimensional compression curve of calcareous sand. Liu et al.²⁸ performed the unidirectional compression test, and demonstrated that calcareous sand has almost no recoverable elastic deformation and the compression process has a significant particle breakage phenomenon. Liao²⁹ investigated the fractal characteristics of calcareous sand particles before and after breakage using a homemade one-dimensional high-pressure consolidation test equipment, and discovered that the relative breakage index is linear with vertical stress and fractal dimension.

Zhang et al.³⁰ conducted confined compression tests on two materials, calcareous sand and quartz sand, and discovered that with the increase in the vertical stress, the particle breakage makes the particles gradually tend to fractal distribution and the ratio of the volumetric strain to the relative breakage index remains unchanged, proposed a mathematical model expression for predicting the variation in the relative breakage index. Xiao et al.³¹ conducted confined compression tests on calcareous sand with vertical pressure ranging from 0.1 to 3.2 MPa, and discovered that the degree of breakage as well as volumetric deformation of calcareous sand is directly proportional to the input work, and the relationship between the former and the input work is independent of the initial density. Coop³² systematically investigated the compression properties of calcareous sands and found that the compression properties of calcareous sands are similar to those of normally consolidated clay, and the compression deformation is dominated by plasticity, which is related to the particle breakage. Cai et al.³³ combined with confined compression tests and found that particle breakage is correlated with stress level and relative density, and established a functional expression between the two. Tong et al.³⁴ discovered that the yield stress decreases with the increase in the saturation in the one-dimensional compression test, the compression index remains almost constant, which is independent of the saturation state. According to the results of triaxial tests, some scholars have proposed dilatancy equations considering the effects of particle breakage³⁵⁻³⁷.

The effects of particle shape on the mechanical properties of calcareous sand is an important topic discussed by researchers. Payan et al.³⁸ analyzed the effects of particle shape on the shear modulus, small-strain damping ratio, and poisson's ratio of granular soils. According to artificial neural network (ANN) models and genetic programming (GP) algorithm, Khodkarii et al.³⁹ simulated the calculation method of the maximum shear modulus of granular soils taking into account the effects of particle shape. Clayton et al.^{40,41} demonstrated that particle shape had a significant effect on the compression and shear properties of granular soils, and proposed a method to define the three-dimensional morphology of particles as well as a new method for determination of gradation. Karabash and Cabalar⁴² investigated the effects of particle shape of sandy soil on improving the mechanical properties of cohesive soil according to triaxial tests.

Previous studies indicated that the research on the compression properties of calcareous sand has achieved relatively rich results. These studies revealed that the study of the mechanical properties of calcareous sand is invariably associated with the particle breakage effects of calcareous sand. However, the tests of calcareous sand in these literatures are basically for the experimental study under a particular breakage index, the variability of different particle breakage indices is not discussed much.

In view of this, in this study, calcareous sand specimens with different initial void ratios and initial particle sizes were designed for confined compression tests. According to the specimen particle analysis test before and after confined compression, the particle size distribution before and after the test were described and compared.

Various breakage indices were accurately calculated according to different breakage measurement methods, and their differences, advantages and disadvantages were compared and analyzed, and universal indices were sought to characterize the particle breakage. The relationship between particle breakage index and macroscopic mechanical properties of specimen was summarized. The test results are expected to provide theoretical guidance for the construction of calcareous sand islands and reefs. The innovations of this paper are as follows: (1) The percentage evolution of fine particles (particle size less than 0.074 mm) of calcareous sand particle gradation under loading was investigated. (2) The advantages and disadvantages of six commonly used quantitative parameters of particle breakage were compared and analyzed, and the relationship between Einav breakage index and Hardin breakage index was emphatically studied.

Specimens and test scheme

Specimen preparation

The test material was calcareous sand from a sea area in southern China. The main chemical composition of the calcareous sand was calcium carbonate (equivalent calcium carbonate content accounted for 96.39%), as determined by X-ray fluorescence spectrometry. The specific gravity of calcareous sand particles was determined to be 2.75 according to the specific gravity bottle method in China's standard for soil test method (YS/T 5225-2016)⁴³. Considering that single-particle-size particles were more fragile and most of the particle sizes were below 2 mm, three gradations were selected for the test, 1–2 mm, 0.5–1 mm and 0.25–0.5 mm. Due to the extremely irregular shape and brittle nature of calcareous sand particles, particle breakage continuously occurred in the sieving process, the amount of sieving retention in the sieving process gradually decreased with the increase in time, and manual sieving was prone to produce non-uniformity and the difference of amplitude and frequency. Therefore, the test strictly controlled the vibrating sieving time to 30 min through determining the relationship between the amount of sieving retention and time, and the calcareous sand was sieved for preparation. The maximum and minimum void ratios of the three gradations and the original gradation are listed in Table 1. Considering the variability between the void ratios of each gradation, the initial void ratios e_0 of the 1–2 mm and 0.5–1 mm gradations were set to 1.10, 1.20 and 1.30, and the initial void ratios e_0 of the 0.25–0.5 mm gradation were set to 1.00, 1.05 and 1.10.

Test scheme

The test apparatus was a WG high-pressure consolidation apparatus produced in Nanjing. The specimen was a cylindrical specimen with a height of 2 cm and a diameter of 6.18 cm, and the maximum loading was 6000 kPa. The high-pressure consolidation apparatus was of steel construction, which was loaded by weights in the form of levers and equipped with a leveling device. The load arm of apparatus was 24:1. The displacement of specimen was measured using a dial gauge. The horizontal bar of the consolidation apparatus was levelled first, and the inner side of the ring cutter with an inner diameter of 6.18 cm and a height of 2 cm was coated with a thin layer of petroleum jelly before being loaded into the consolidation apparatus, and then the prepared sand specimens were uniformly loaded into the ring cutter in three layers with a funnel. The specimen preparation and loading process of the test were implemented in accordance with the industrial standard of the People's Republic of China, Specification for soil test (YS/T 5225-2016)⁴³. Pre-compression at a tiny pressure was carried out before the test, and the tiny pre-compression loading was empirically determined to be 1 kPa. The loading was two graded loading and one graded unloading. Test loading ratio and unloading ratio were 1. The initial test was loaded to a maximum of 2 MPa and began to unload to 0.4 MPa and then to load to 6 MPa. Dial indicator readings were taken every 10 min after each stage of loading. If the dial indicator reading changed within the range of 0.005 mm within 10 min, it was considered that the loading was stable, and the next loading can be conducted. Particle analysis tests were performed after carefully removing the specimens after each stage of loading, and various particle breakage indices were calculated. Particles with particle size larger than 0.1 mm were determined by sieving analysis method, and particles with particle size smaller than 0.1 mm were determined by laser scattering method. 3 groups of specimens were loaded with 11 levels, so the total number of specimens was 33.

Results and discussion

Figure 1 displays the compression curves of three single-particle-size group specimens under the same loading path with three different initial void ratios. For specimens with different initial void ratios, the compression curves of the same specimens gradually converged to a common straight line with the increase in the pressure P , which was most obvious in the single-particle-size group specimens of 0.25–0.5 mm. This indicated that with the increase in the pressure, the proportion of compression characteristics controlled by the initial void ratio gradually decreased. The convergence to a straight line was less pronounced for the 1–2 mm and 0.5–1 mm single-particle-size groups specimens than for the 0.25–0.5 mm single-particle-size group specimens. This is mainly because the two groups of particles in the normal stress level produced more obvious particle breakage, the compression characteristics of the specimen are controlled by a combination of particle breakage and particle rearrangement, and the proportion of compression properties controlled by particle breakage gradually

Particle size (mm)	2–1 mm	1–0.5 mm	0.5–0.25 mm
Maximum void ratio e_{\max}	1.453	1.336	1.200
Minimum void ratio e_{\min}	0.763	0.760	0.725

Table 1. Maximum and minimum void ratios of calcareous sand under different particle sizes.

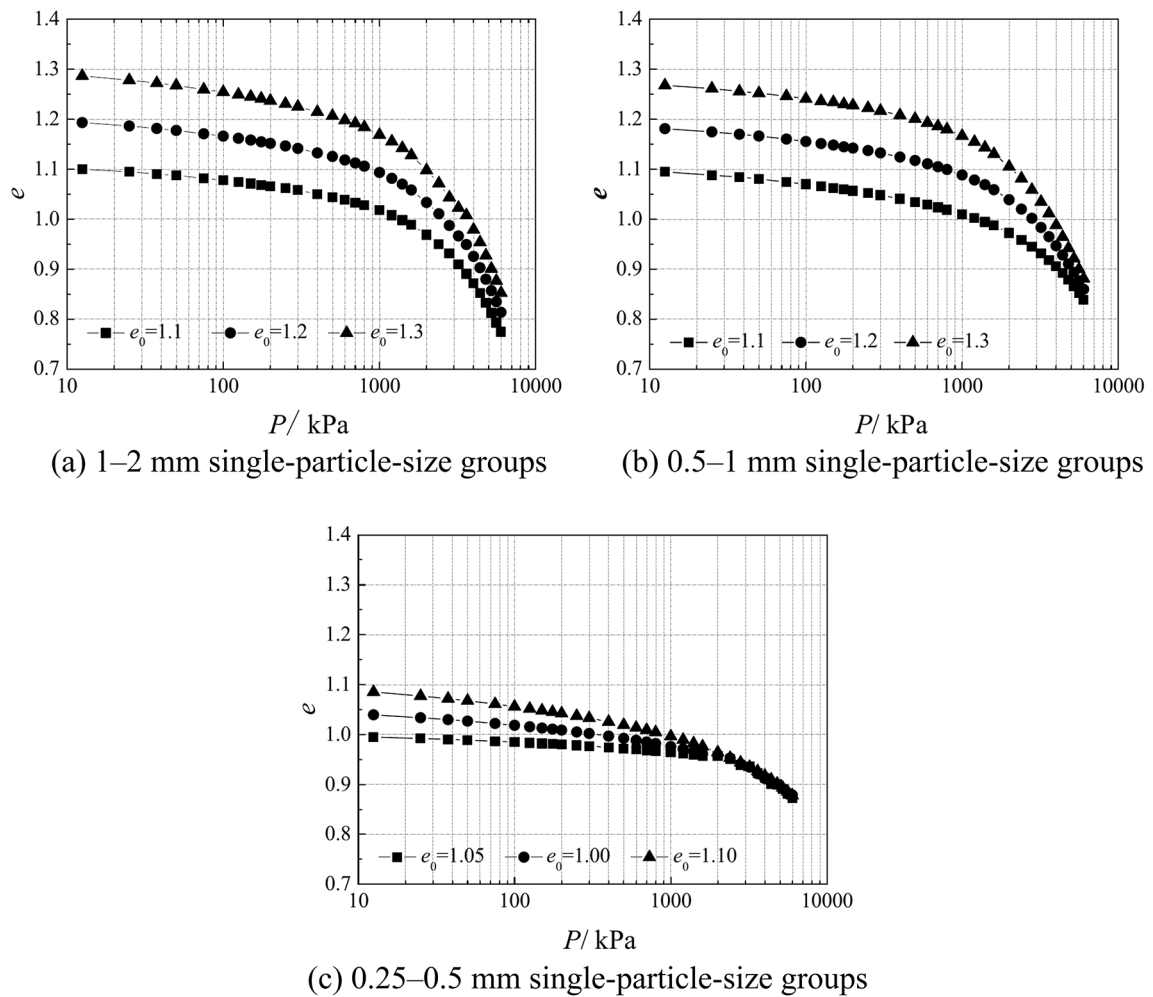


Fig. 1. Compression curves of calcareous sand.

increased with the increase in the pressure. For the relatively loose specimens with large initial void ratios, the variation in the void ratio was larger in the early stage of loading, the compression coefficient was also larger, and the compression curve in the initial stage was steeper. For the relatively dense specimens with little initial void ratios, the variation in the void ratio was smaller in the early stage of loading, the compression coefficient was also smaller, and the compression curve in the initial stage was more gentle.

Figure 2 displays the typical loading–unloading–reloading curves of each single-particle-size group specimen. The unloading rebounds of all types of specimens were small, which indicated that the deformation occurring during compression of calcareous sand particles aggregates was mainly plastic deformation with irreversibility or irrecoverability. This is mainly because in the unloading process, the contact mode between particles remained basically unchanged. After unloading, the contact stress between particles decreased so as to produce a considerably weak particle rearrangement. Under the test stress level, the particle breakage was an irreversible process, the particles were unlikely to recover the original state before breakage, the mutual position of the particles did not change greatly after breakage, so the rebound was very small. Moreover, the reloading process of each specimen basically followed the original path. This is mainly because the contact stress between the particles gradually increased with the increase in the pressure. The contact stress between particles did not produce new particle breakage until the stress level at unloading was reached. When the pressure was further increased to the level before unloading, the contact stress between the particles furtherly increased, and some particles subjected to contact stresses by neighboring particles reached the particle strength, leading to more particle breakage and rearrangement, and thus producing a more pronounced yield point, i.e., the stress level at the time of the original unloading.

Figure 2 displays the comparison of compression curves when the initial void ratio of each single-particle-size group specimens is 1.1. If no particle breakage in each specimen, when the initial void ratios were the same, the specimens with larger particle size were considered to be the most compact and less compressible, while the specimens with smaller particle sizes were considered to be more loose and more compressible. However, the actual situation was that each specimen were loaded to 6000 kPa, the compression of the specimen with larger particle size was larger, and the compression of the specimen with smaller particle size was smaller. Obviously,

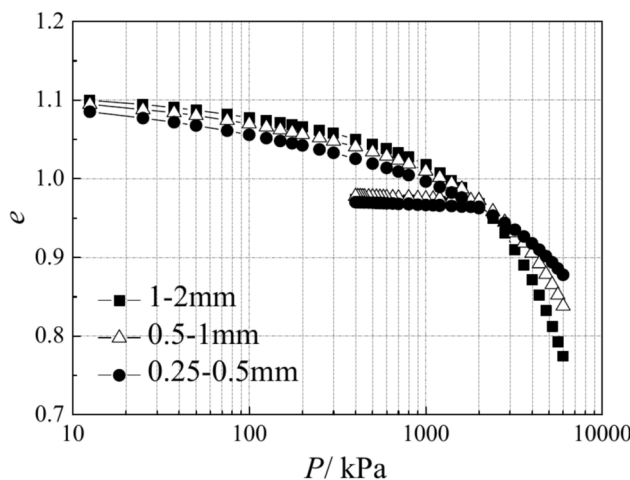


Fig. 2. Loading–unloading–reloading curves of calcareous sand.

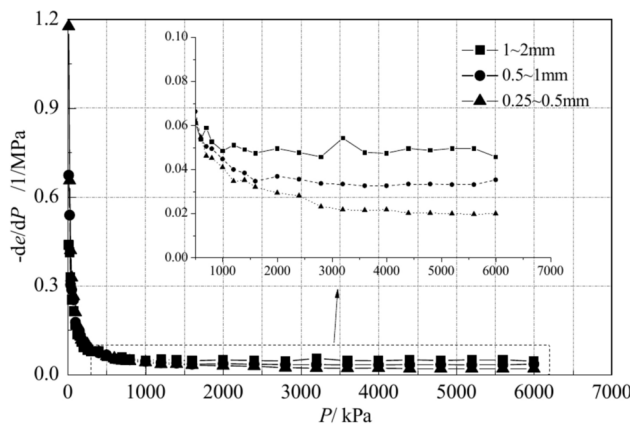


Fig. 3. $(-de/dP)-P$ curve.

during the compression of calcareous sand, the compression characteristics were not only controlled by gas extrusion and particle rearrangement mechanisms, but also by particle breakage.

To further compare and analyze the variation in vertical strain of each specimen during the compression process, the $(-de/dP)-P$ curve is plotted in conventional coordinates by taking the negative value of the void ratio e after derivation of the pressure P , as depicted in Fig. 3. The decreasing rate of void ratio of each specimen decreased with the increase in the pressure, which indicated that the decreasing trend of void ratio slowed down with the increase in the pressure. At the beginning of loading, the decreasing rate of the void ratio of the smaller particle size group was larger, and the decreasing trend of the void ratio was more drastic. The enlarge image within the coordinates of the dashed rectangle box in Fig. 3 revealed that after loading to a certain extent, the decreasing rate of the void ratio of the smaller particle size group was smaller, indicating that the decreasing trend of the void ratio was more gentle, and the decreasing rate of void ratio of the larger particle size group was greater, indicating that the decreasing trend of void ratio was more drastic.

The above phenomena more fully illustrated that the particle breakage mechanism and the gas extrusion and particle rearrangement mechanism jointly controlled the compression characteristics of calcareous sand in the compression process. At the beginning of loading, the proportion of gas extrusion and particle rearrangement controlling the compression characteristics was larger as the major factor, and the proportion of particle breakage was smaller as the minor factor. With the increase in the pressure, the void ratio gradually decreased, the proportion of gas extrusion and particle rearrangement controlling the compression characteristics gradually decreased, and the proportion of particle breakage and particle rearrangement increased. Particle breakage and particle rearrangement mechanisms became the main factors controlling the compression characteristics of calcareous sand.

Particle breakage analysis

Figure 4 displays the gradation curves of each specimen under various levels of loading in double logarithmic coordinates. The gradation curves of various types of single-particle-size group specimens produced different

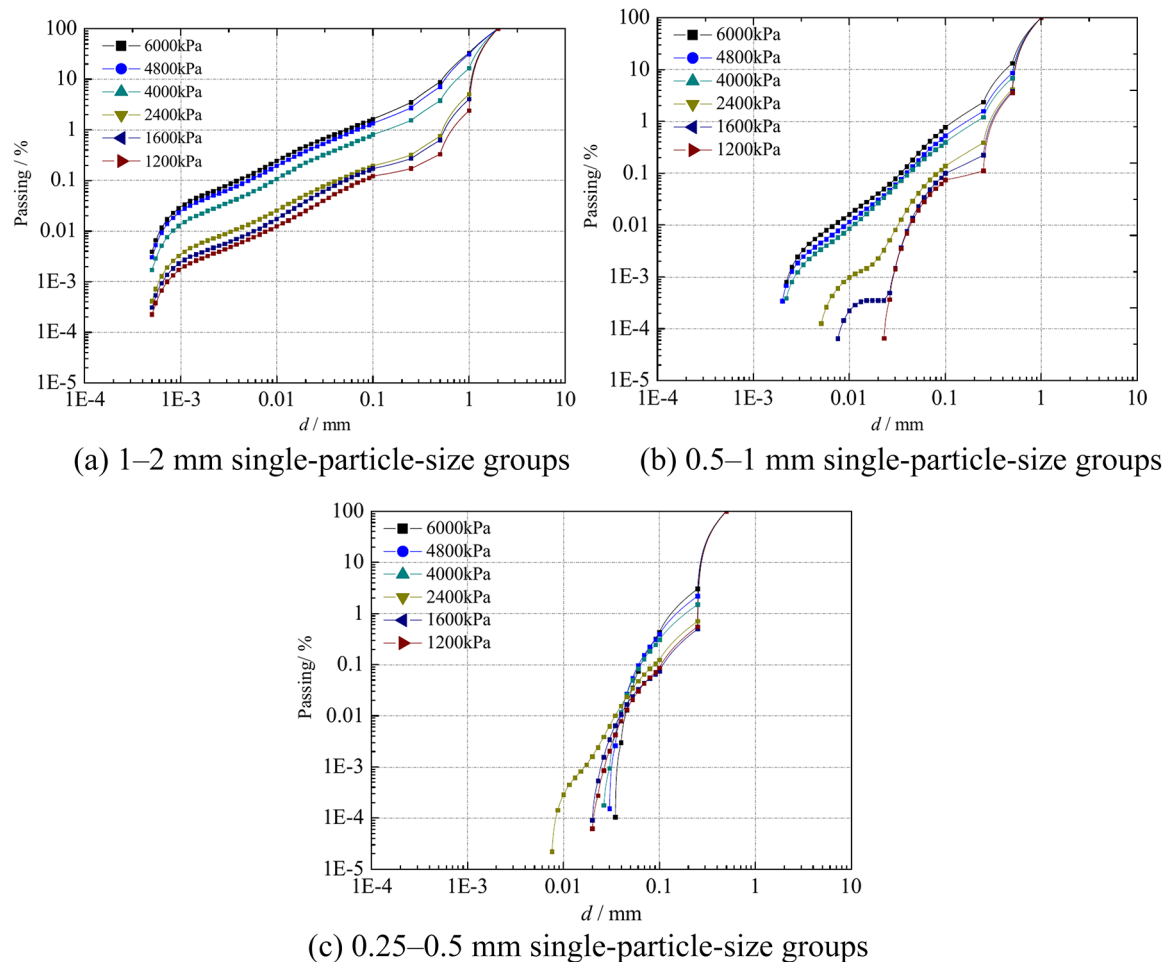


Fig. 4. Gradation curves of different particle size groups under different loadings (double logarithmic coordinates).

degrees of changes before and after the test loading was applied. For all types of specimens, with the increase in the loading, the particle breakage of the specimens increased, the particle content of large particle size decreased, the particle content of small particle size increased, and some particles with a particle size less than 0.074 mm were produced, some even as small as 0.479 μm , which was obviously due to the abrasion or breakage of the particles. The particle size of the specimens was larger, the particle breakage was larger, which indicated that under the same loading, the particle size was larger, the possibility of particle breakage was higher and the particle breakage was larger.

As depicted in Fig. 4, the specimens of each single-particle-size group produced fine particles with particle size less than 0.074 mm under different loadings, and the smallest particles present in the specimens tended to decrease with the increase in the loading. Notably, for 0.25–0.5 mm single-particle-size group specimens, minimum particle sizes produced under some small loadings was smaller than that under large loadings. The reason is that the amount of fine particles produced by this specimen under the test loading was extremely small, easily leading to errors in the laser scattering test, but the overall trend of the phenomenon illustrated above was consistent. Meanwhile, for the specimen with larger particle size, the particle size of the smallest particles was smaller under the same loading. On the contrary, for the specimen with smaller particle size, the particle size of the smallest particles was larger.

According to the fitted interpolated data to calculate the various particle breakage indices, the characteristic particle sizes of each specimen after compression were used to calculate the relevant particle breakage indices B_{10} , B_{15} , B_{50} , B_M and B_r . The calculated various breakage indices are summarized in Fig. 5. For the characteristic particle size breakage indices such as B_{10} , B_{15} and B_{50} , the integrity of the gradation curve was not adequately represented. For a single-particle-size group of 0.25–0.5 mm, the value of B_{10} was zero under the loading of 200 kPa, and the value of B_{50} was zero under the loading of below 2400 kPa, which did not reflect the particle breakage, the corresponding gradation curves were changed, indicating that these indices were not convincing. For B_M , the breakage data of three different single-particle-size groups revealed that although the B_M indices of all specimens were not zero with the increase in the loading. However, the definition of B_M indicated that its value had no upper limit, which was not conducive to the comparison of particle breakage of different specimens. As depicted in Fig. 5, with the increase in the loading, all types of particle breakage index presented

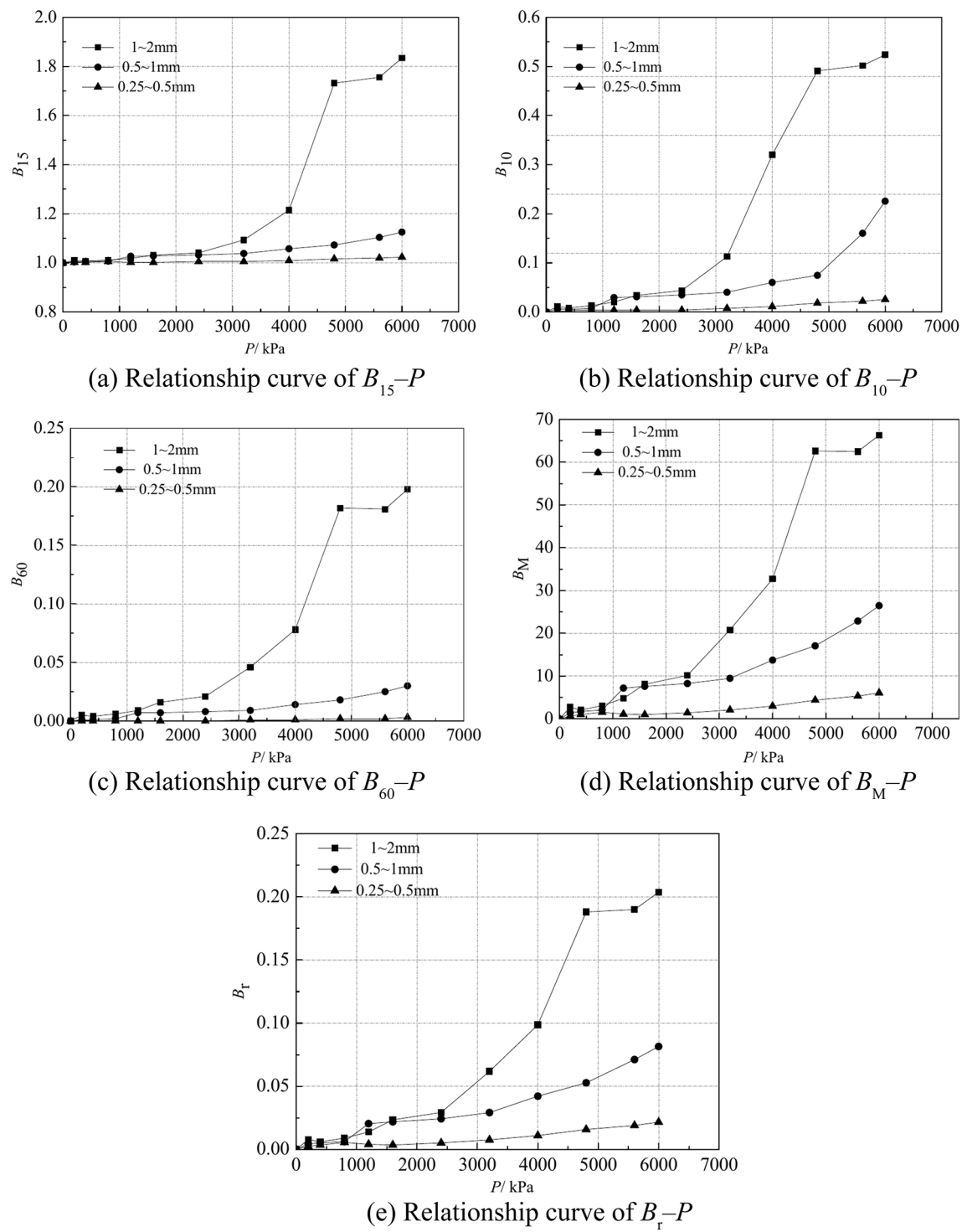


Fig. 5. Particle breakage indices of different particle size groups under different loadings.

an increasing trend, and the particle size of the specimen was larger, the value of the breakage index was greater. However, according to the above analysis, in this study, Hardin relative breakage index B_r was used for the metric of particle breakage.

According to Fig. 5, after tracing the data of the relative breakage index B_r and the corresponding loading P in the specimens of each single-particle-size group, the relationship between the relative breakage index B_r and the pressure P can be obtained by function fitting, as displayed in Fig. 6. The fitted functional relationship of B_r-P can be approximated using Eq. (1), where parameters a , b and c are all greater than zero.

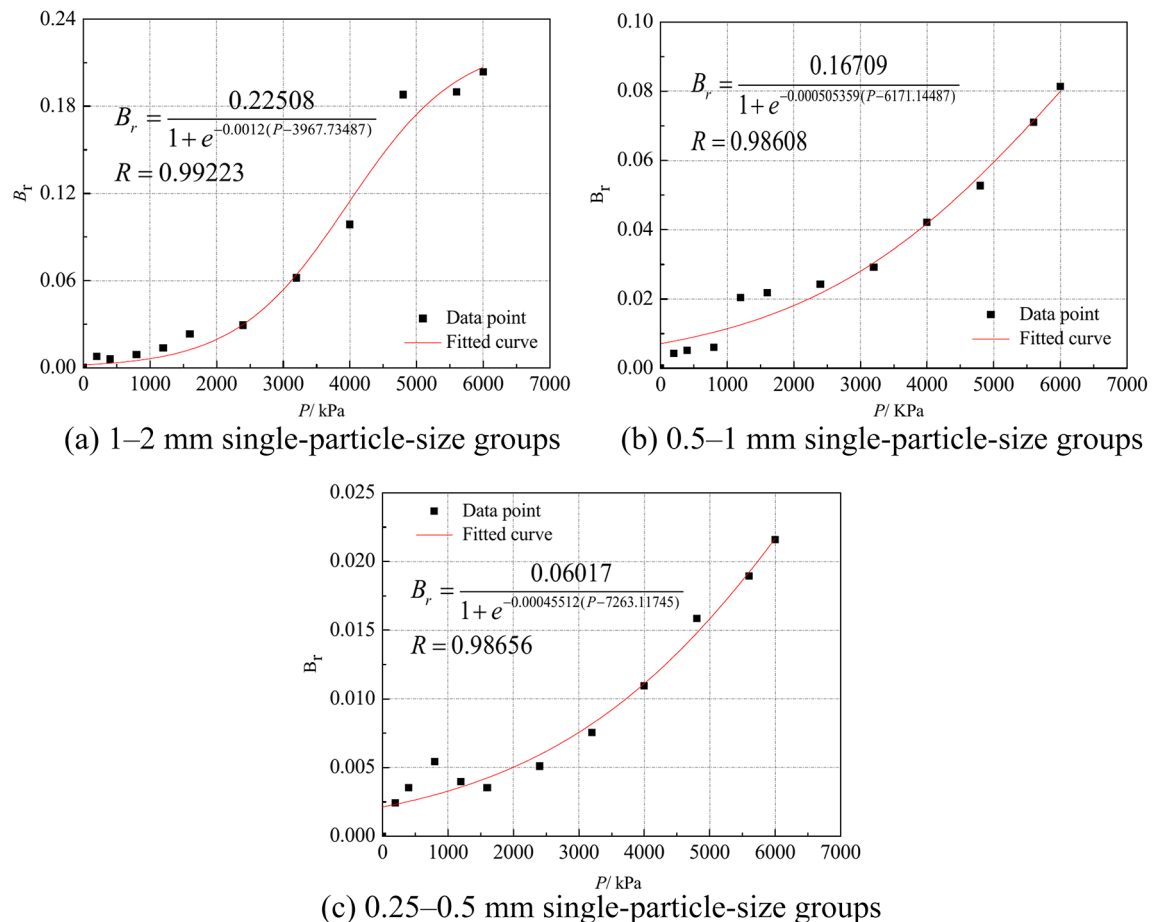


Fig. 6. Relationship curve of B_r versus P .

$$B_r = \frac{a}{1 + e^{-b(P-c)}} \quad (1)$$

where P is the independent variable, B_r is the dependent variable, and the parameters a , b and c are all greater than zero. To know the physical significance of the specific parameters, the analysis is as follows:

Equation (2) is the first-order derivative of Eq. (1) for the pressure.

$$\frac{dB_r}{dP} = \frac{abe^{-b(P-c)}}{[1 + e^{-b(P-c)}]^2} > 0 \quad (2)$$

The relative breakage index B_r was a monotonically increasing function of the pressure P . With the increase in the loading, the particle breakage of the specimen increased. The second-order derivative of Eq. (1) for pressure P or the first-order derivative of Eq. (2) for pressure P yields Eq. (3) as follows:

$$\frac{d^2 B_r}{dP^2} = \frac{ab^2 e^{-b(P-c)} [e^{-b(P-c)} - 1]}{[1 + e^{-b(P-c)}]^3} \quad (3)$$

From the analysis of Eq. (3), only when $P=c$, $d^2 B_r/dP^2=0$, was the inflection point, when $0 < P < c$, B_r increased with the increase in P , and the increasing trend was stronger, when $P > c$, B_r increased with the increase in P , but the increasing trend slowed down. When $P=c$, B_r increased most sharply with the increase in P . Some scholars vaguely defined the crushing stress of the specimen as the stress corresponding to a sudden variation in the compression coefficient in the compression curve. However, in the compression curves of some specimens, the sudden variation in the compression coefficient was not very obvious. For example, when the initial void ratio was relatively large, the effect of the void ratio was not eliminated when the specimen reached the crushing stress. The value range for the sudden variation in compression coefficient was not clearly defined, and the values of the sudden variation in compression coefficient were different for various specimens. Therefore, the physical significance of particle breaking stress cannot be reflected.

Particle size group (mm)	intermediate particle size d_{50} (mm)	Crushing stress P^0 (kPa)	Ultimate relative breakage index B_r^{\max}
1–2	1.5	1983.867	0.22508
0.5–1	0.75	3085.572	0.16709
0.25–0.5	0.375	3631.559	0.06017

Table 2. Summary of intermediate particle size, crushing stress and ultimate relative breakage index for each particle size group.

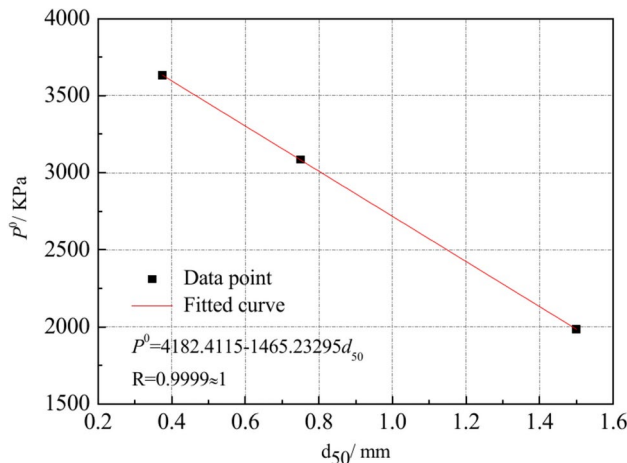


Fig. 7. Relationship curve of d_{50} versus P^0 .

The Slogistic model is now used in physical–chemical tests, bioengineering and other scientific fields, and its functional equation can be expressed as Eq. (1). The function definition domain is $(0, +\infty)$, and the value domain is $(0, a]$. The Slogistic function is also a significant functional relationship for the above B_r – P . According to the analysis in the previous section, the Slogistic function can be divided into three segments: $(0, c/2]$, $[c/2, c]$ and $[c, +\infty)$.

(1) Breakage asymptotic section: in the $(0, c/2]$ section, B_r increased with the increase in P . When x reached $c/2$, B_r surged, at this time the value of y was the crushing stress. (2) Breakage surge section: in the $[c/2, c]$ section, B_r increased more dramatically with the increase in P , and when P reached c , B_r increased most dramatically. (3) Breakage yield section: in the $[c, +\infty)$ section, B_r increased slowly with the increase in P , and tended to the limiting value of a .

The crushing stress level of a specimen is defined as the stress level that corresponds to the surge in particle breakage with the increase in loading. According to the Slogistic model, the value of $c/2$ is determined to be the crushing stress of the particle breakage of the particle size group specimen calcareous sand.

When $P \rightarrow \infty$, Eq. (4) is obtained from Eq. (3).

$$\lim_{P \rightarrow \infty} B_r = a = B_r^{\max} \quad (4)$$

As depicted in Eq. (4), the parameter a is the limiting value of the Hardin relative breakage index B_r^{\max} of specimen.

The intermediate particle size d_{50} of each particle group was taken, that is, 1.5 mm, 0.75 mm and 0.375 mm. According to the above analysis, the intermediate particle size, crushing stress and ultimate relative breakage index of each specimen are summarized in Table 2.

The relationship between the intermediate particle size d_{50} and the crushing stress P^0 and the ultimate relative breakage index B_r^{\max} were plotted and fitted, as displayed in Figs. 7 and 8. The intermediate particle size d_{50} was larger, the crushing stress P^0 was smaller, and the two showed an extremely significant linear relationship. When the pressure was the same, the particle size was larger, the ultimate relative breakage index was larger, and the intermediate particle size d_{50} and the ultimate relative breakage index B_r^{\max} existed a significant semi-log linear relationship.

The relationship between the relative breakage index B_r of Hardin¹⁰ and the relative breakage index B_e of Einav¹¹ is plotted in Fig. 9, where the corresponding areas of the filled regions are S1, S2, S3, S4, and S5, respectively.

According to Fig. 9, the forms of various parameters between Hardin relative breakage index B_r and Einav relative breakage index B_e are obtained, as displayed in Eqs. (5) to (10).

$$B_P = S1 + S2 + S3 \quad (5)$$

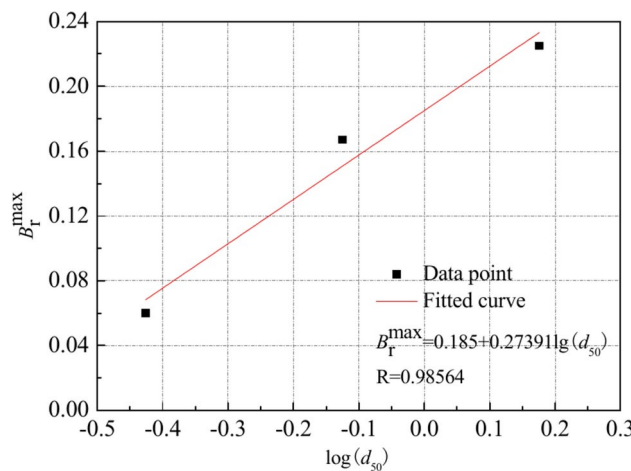


Fig. 8. Relationship curve of d_{50} versus B_r^{\max} .

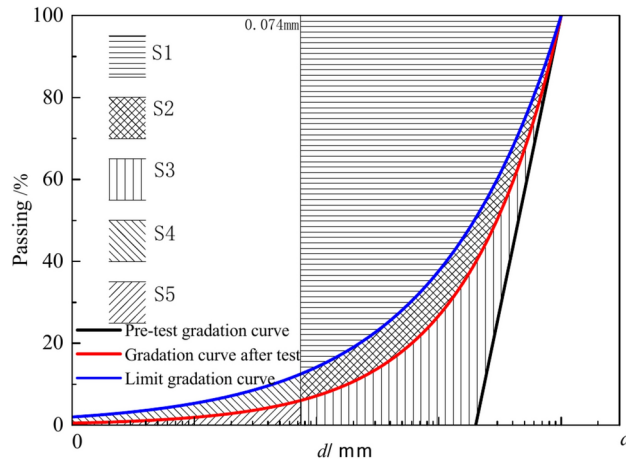


Fig. 9. Comparison of B_r versus B_e .

$$B_t = S3 \quad (6)$$

$$B_r = \frac{B_t}{B_P} = \frac{S3}{S1 + S2 + S3} \quad (7)$$

$$B'_P = S2 + S3 + S4 + S5 \quad (8)$$

$$B'_t = S3 + S5 \quad (9)$$

$$B_e = \frac{B'_t}{B'_P} = \frac{S3 + S5}{S2 + S3 + S4 + S5} \quad (10)$$

where B_p , B_P , B'_t and B'_P are Hardin breakage potential, Hardin total breakage potential, Einav breakage potential and Einav total breakage potential, respectively. According to the analysis of Eq. (5) to Eq. (10):

For B_t and B'_t since $S3 < S3 + S5$, it is obvious that $B_t < B'_t$; while for B_p and B'_P , generally, assuming that $S1 > S4 + S5$, so $S1 + S2 + S3 > S2 + S3 + S4 + S5$, that is, $B_p > B'_P$. Therefore, for B_r and B'_e , the molecule B_t of B_r was smaller than the molecule B'_t of B'_e while the denominator B_p of B_r was larger than the denominator B'_P of B'_e . Thus, in general, the following equation is deduced.

$$B_r < B_e \quad (11)$$

and

Loading	$B_t = S3$	$S1 + S2$	$S5$	$B_t = S3 + S5$
6000	29.04162	113.5584	1.36847	30.41009
5600	27.08399	115.516	1.201544	28.28553
4800	26.81485	115.7852	1.082782	27.89763
4000	14.0683	128.5317	0.627996	14.6963
3200	8.813142	133.7869	0.381236	9.194378
2400	4.177039	138.423	0.156922	4.333961
1600	3.331579	139.2684	0.134703	3.466282
1200	1.96885	140.6312	0.089769	2.058619
800	1.269202	141.3308	0.078509	1.347711
400	0.847471	141.7525	0.04489	0.892361
200	1.097635	141.5024	0.044895	1.14253

Table 3. 1–2 mm particle size group.

Loading	$B_t = S3$	$S1 + S2$	$S5$	$B_t = S3 + S5$
6000	5.50839344	62.14160656	0.612721	6.12111444
5600	4.80993781	62.84006219	0.590174	5.40011181
4800	3.56778822	64.08221178	0.406358	3.97414622
4000	2.85125837	64.79874163	0.328075	3.17933337
3200	1.97024329	65.67975671	0.296007	2.26625029
2400	1.64083531	66.00916469	0.102541	1.74337631
1600	1.47925123	66.17074877	0.079053	1.55830423
1200	1.37692641	66.27307359	0.056523	1.43344941
800	0.41154319	67.23845681	0.056057	0.46760019
400	0.35052852	67.29947148	0.044862	0.39539052
200	0.28946916	67.36053084	0.044851	0.33432016

Table 4. 0.5–1 mm particle size group.

Loading	$B_t = S3$	$S1 + S2$	$S5$	$B_t = S3 + S5$
6000	0.65044626	29.49955374	0.328034	0.97848
5600	0.57106367	29.57893633	0.292757	0.863821
4800	0.47720634	29.67279366	0.282368	0.759574
4000	0.32978855	29.82021145	0.225671	0.55546
3200	0.22754673	29.92245327	0.146831	0.374378
2400	0.15383087	29.99616913	0.090649	0.24448
1600	0.10673662	30.04326338	0.056656	0.163393
1200	0.11978999	30.03021001	0.067634	0.187424
800	0.16424093	29.98575907	0.067302	0.231543
400	0.10685841	30.04314159	0.044862	0.15172
200	0.07363603	30.07636397	0.033638	0.107274

Table 5. 0.25–0.5 mm particle size group.

$$B_e = \frac{S3 + S5}{S2 + S3 + S4 + S5} > \frac{S3 + S5}{S1 + S2 + S3} > \frac{S3}{S1 + S2 + S3} = B_r \quad (12)$$

$S1 + S2$, $S3$ and $S5$ were obtained from the data analyzed by the test particles. Since the particle termination gradation curve was still an unknown gradation, $S4$ cannot be calculated and $S1$ and $S2$ cannot be calculated separately according to the test data in this study. Therefore, $S1 + S2$, $S3$ and $S5$ were calculated separately for various specimens in this study and summarized in Tables 3, 4 and 5.

After tracing the data of B_t and the logarithmic value $\lg P$ of the corresponding loading under each loading for single-particle-size group specimens, the relationship between B_t and $\lg P$ was obtained through function fitting, as displayed in Fig. 10.

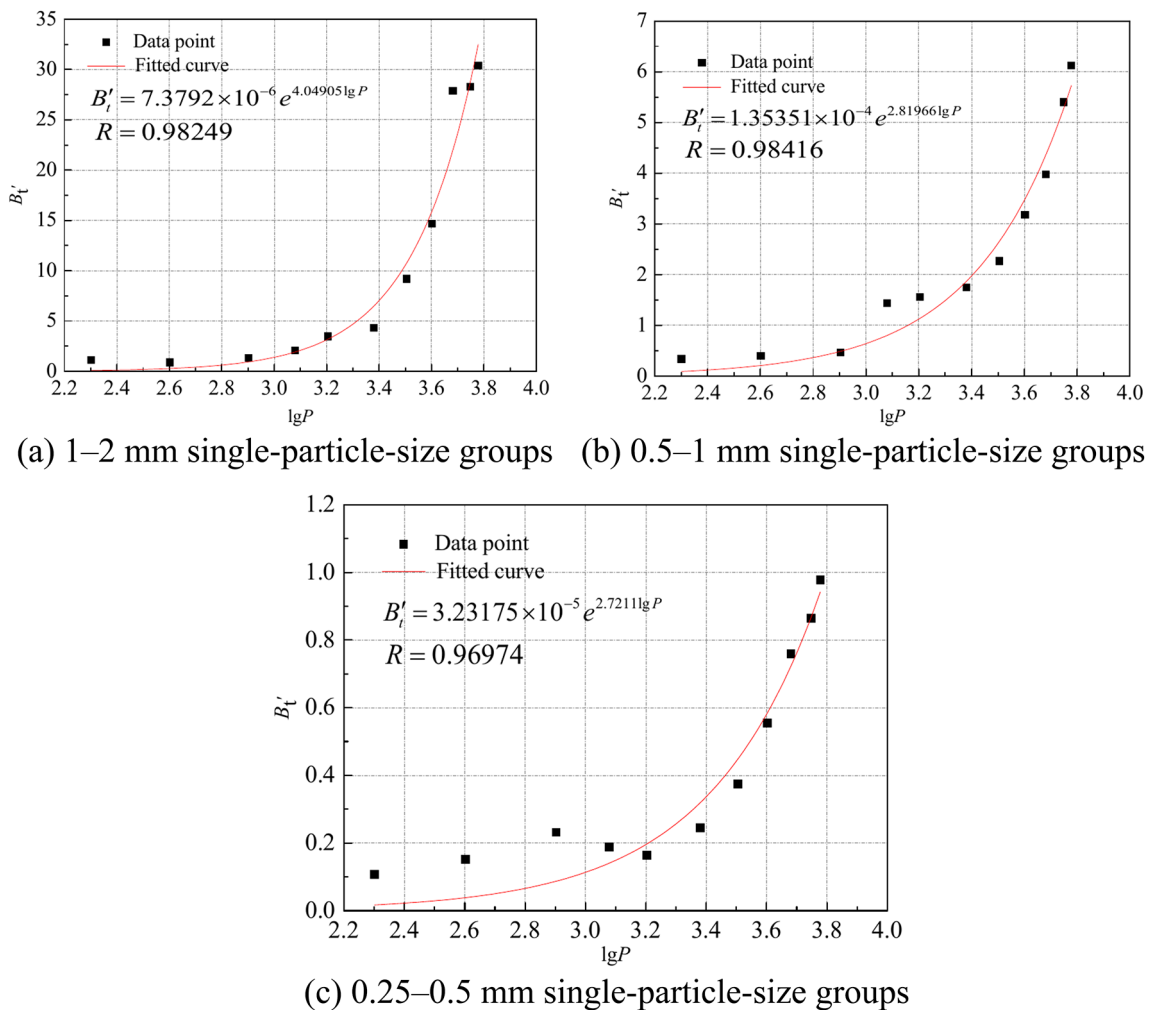


Fig. 10. Relationship between B'_t and $\lg P$.

As depicted in Fig. 10, B'_t and $\lg P$ existed a significant exponential function relationship, which implied that an intrinsic connection between the two. After tracing the data of S3 and the logarithmic value $\lg P$ of the corresponding loading under each loading for single-particle-size group specimens, the relationship between S3 and $\lg P$ was obtained through function fitting, as displayed in Fig. 11. S5 and $\lg P$ existed a more significant exponential function relationship, and the correlation coefficient was higher than that between B'_t and $\lg P$, and the connection was more obvious. Therefore, S5 can also be used as a measure of particle breakage and has some application prospects.

Conclusions

1. For specimens with different initial void ratios, the compression curves of the similar specimens gradually converged to a common straight line with the increase in the pressure P . The deformation of calcareous sand particle aggregates during the compression process was mainly plastic deformation, which was irreversible or irrecoverable. In the compression process of calcareous sand, the compression characteristics were not only controlled by the gas extrusion and particle rearrangement mechanism, but also by the occurrence of various degrees of particle breakage.
2. Under the same loading, the particle size of the specimen was larger, the probability of particle breakage was higher, and the amount of particle breakage was larger. With the increase in the loading, the presence of particle size less than 0.074 mm in the specimen presented a decreasing trend, all types of particle breakage indices presented an increasing trend. The particle size of the specimen was larger, the value of the breakage index was larger. Comparative analysis revealed that the use of Hardin relative breakage index B_r for the metric of particle breakage had better applicability.
3. Based on the analysis of the test results, the Hardin relative breakage index B_r and the pressure P existed an extremely significant correlation. The parameter a represents the Hardin ultimate relative breakage index, and the value of parameter $c/2$ represents crushing stress of the specimen. The intermediate particle size d_{50} of the specimen was larger, the crushing stress P^0 was smaller, and the two showed an extremely significant

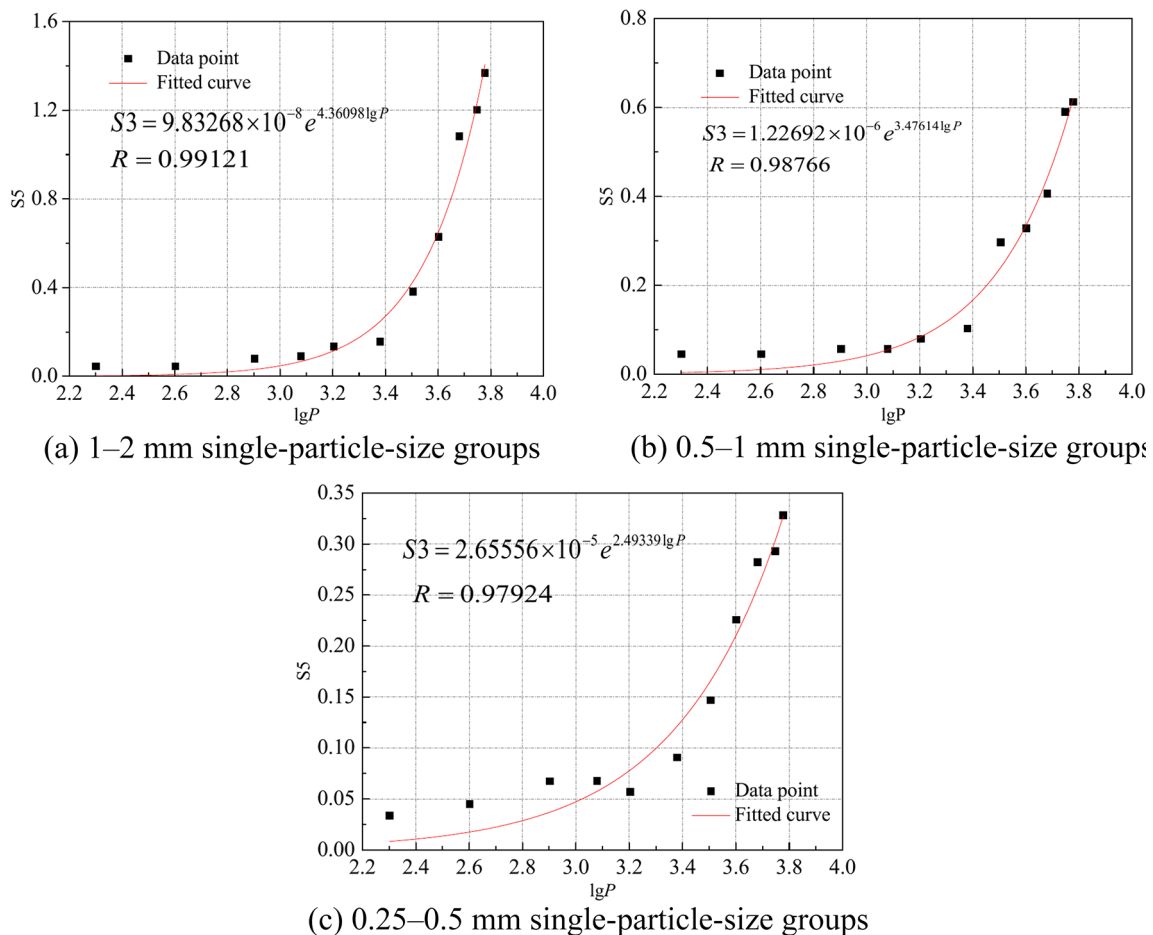


Fig. 11. Relationship between S_5 and $\lg P$.

linear relationship. When the pressure was the same, the particle size was larger, the ultimate relative breakage index was larger, and the intermediate particle size d_{50} and the ultimate relative breakage index B_r^{max} existed a significant semi-log linear relationship. Einav crushing potential B'_t had a significant exponential function relationship with $\lg P$. A more significant exponential function relationship existed between parameter S_5 and $\lg P$ than between B'_t and $\lg P$. Therefore, S_5 can also be used as a measure of particle breakage and has some application prospects.

Notably, so far researchers have proposed numerous particle breakage indices, which cannot be compared comprehensively. Only six representative indices were selected for testing in this paper. Moreover, although a single gradation is selected to minimize the effects of particle shape on particle breakage, the existence of particle shape differences among different particle sizes should not be ignored, which will also cause some errors in the test results. Furthermore, in this paper, the repeated specimen preparation method for the test cannot guarantee the consistency of each specimen, which is still a problem that needs to be further investigated.

Data availability

The data of this study are available from the corresponding author upon request.

Received: 22 July 2024; Accepted: 14 January 2025

Published online: 22 January 2025

References

1. Soroush, A. & Jannatiaghdam, R. Behavior of rockfill materials in triaxial compression testing. *Int. J. Civ. Eng.* **10**(12), 153–161 (2012).
2. Chen, Q. L. et al. Mechanical behavior and particle crushing of irregular granular material under high pressure using discrete element method. *Sci. Rep.* **13**, 7843 (2023).
3. Xu, D. S., Chen, W. & Fan, X. C. Experimental investigation of particle size effect on the self-healing performance of microcapsule for cemented coral sand. *Constr. Build. Mater.* **256**, 119343 (2020).
4. Wang, X., Zhu, C. Q. & Wang, X. Z. Experimental study on the coefficient of lateral pressure at rest for calcareous soils. *Mar. Georesour. Geotechnol.* **38**(8), 989–1001 (2020).
5. Miura, N. & O-Hara, S. Particle crushing of decomposed granite soil under shear stresses. *Soil Found.* **19**(3), 1–14 (1979).

6. Marsal, R. J. Large-scale testing of rockfills materials. *J. Soil Mech. Found. Eng. ASCE* **93**(2), 27–43 (1967).
7. Lee, K. L. & Seed, H. B. Drained strength characteristics of sands. *J. Soil Mech. Found. Div.* **6**(5), 117–141 (1967).
8. Lade, P. V., Yamamoto, J. A. & Bopp, P. A. Significance of particle crushing in granular materials. *J. Geotech. Eng. ASCE* **122**(4), 309–316 (1996).
9. Zhang, B.W. *Particle Breakage Research of Calcareous Sand Under Confined Compression*. Master's thesis, Wuhan University of Technology (2014).
10. Hardin, B. O. Crushing of soil particles. *J. Geotech. Eng. ASCE* **111**(10), 1177–1192 (1985).
11. Einav, I. Breakage mechanics-part I: Theory. *J. Mech. Phys. Solids* **55**(6), 1274–1297 (2007).
12. Wang, W. W. et al. An Image-based method for evaluating changes in particle size and morphology distributions of aggregate materials after vibratory compaction test. *Constr. Build. Mater.* **430**, 136483 (2024).
13. Luo, M. X., Liu, X. X., Zhong, L., Wang, X. X. & Wu, C. Effects of particle breakage on the mechanical behavior of calcareous sand under confined compression tests. *Int. J. Civ. Eng.* **22**, 1–18 (2024).
14. Hagerty, M. M., Hite, D. R., Ullrich, C. R. & Hagerty, D. J. One-dimensional high-pressure compression of granular media. *J. Geotech. Eng.* **119**(1), 1–18 (1993).
15. Liu, X. X. et al. Experimental study on the effects of water content on the compression characteristics and particle breakage of calcareous sand. *Sci. Rep.* **14**, 6853 (2024).
16. Miao, G. & Airey, D. Breakage and ultimate states for a carbonate sand. *Geotechnique* **63**, 1221–1229 (2013).
17. McDowell, G. R. On the yielding and plastic compression of sand. *Soils Found.* **42**(1), 139–145 (2002).
18. Lv, Y., Liu, J. & Xiong, Z. One-dimensional dynamic compressive behavior of dry calcareous sand at high strain rates. *J. Rock Mech. Geotech. Eng.* **11**(1), 192–201 (2019).
19. Nakata, Y., Hyodo, M., Hyde, A. F. L., Kato, Y. & Murata, H. Microscopic particle crushing of sand subjected to high pressure one-dimensional compression. *Soils Found.* **41**(1), 69–82 (2001).
20. Yamamoto, J. A., Bopp, P. A. & Lade, P. V. One-dimensional compression of sands at high pressures. *J. Geotech. Eng.* **122**, 147–154 (1996).
21. Peng, Y., Ding, X., Xiao, Y., Deng, X. & Deng, W. Detailed amount of particle breakage in nonuniformly graded sands under one-dimensional compression. *Can. Geotech. J.* **57**, 1239–1246 (2020).
22. Ding, H. H. et al. Particle breakage and its mechanical response in granular soils: A review and prospect. *Constr. Build. Mater.* **409**, 133948 (2023).
23. Yao, T., Xing, X. & Li, W. Evolution of particle morphology of quartz sand during one-dimensional compression. *Powder Technol.* **429**(1), 118921 (2023).
24. Altuhafi, F. N. & Coop, M. R. Changes to particle characteristics associated with the compression of sands. *Geotechnique* **61**(6), 459–471 (2011).
25. Aghajani, H. F., Salehzadeh, H. & Rezvani, R. Energy equilibrium during crushing of sandy soils under isotropic compression. *Arab. J. Sci. Eng.* **41**(4), 1531–1542 (2016).
26. Yang, Y., Zhang, C., Wang, R., Jiang, M. & Tian, Y. Engineering properties of the compressibility and crushing characteristics of transitional soils mixed with silicate and carbonate sands. *Eng. Geol.* **292**, 106246 (2021).
27. Pestana, J. M. & Whittle, A. Compression model for cohesionless soils. *Geotechnique* **45**(4), 611–631 (1995).
28. Liu, C. Q., Yang, Z. Q. & Wang, R. The present condition and development in studies of mechanical properties of calcareous soils. *Rock Soil Mech.* **16**(4), 74–84 (1995).
29. Liao, X. H. *Compressibility and Crushing of Calcareous Sand in High Confined Compression*. Master's thesis, Wuhan University of Technology (2015).
30. Zhang, J. R., Zhang, B. W., Hu, Y. & Liao, X. H. Predicting the particle breakage of granular geomaterials. *Chin. J. Rock Mech. Eng.* **35**(9), 1898–1905 (2016).
31. Xiao, Y. et al. Particle breakage and deformation of carbonate sands with wide range of densities during compression loading process. *Acta Geotech.* **12**(5), 1177–1184 (2017).
32. Coop, M. R. The mechanics of uncemented carbonate sands. *Geotechnique* **40**(4), 607–626 (1990).
33. Cai, Z. Y. et al. Experimental study on the influence of density and stress level on particle breakage of coral sand. *J. Hydraul. Eng.* **50**(2), 184–192 (2019).
34. Tong, C. X., Burton, G. J., Zhang, S. & Sheng, D. Particle breakage of uniformly graded carbonate sands in dry/wet condition subjected to compression/shear tests. *Acta Geotech.* **15**(9), 2379–2394 (2020).
35. Du, J., Xiong, Z. M., Shen, X. G. & Li, C. C. Experimental study on the effect of coarse grain content on the dilatancy and particle breakage characteristics of coarse-grained soils. *Fractal Fract.* **8**(2), 1–17 (2023).
36. Ozbay, A. & Cabalar, A. F. Effects of triaxial confining pressure and strain rate on stick-slip behavior of a dry granular material. *Granul. Matter* **18**, 60 (2016).
37. Wu, E. L., Zhu, J. G., He, S. B. & Peng, W. M. A stress dilatancy relationship for coarse-grained soils incorporating particle breakage. *Granul. Matter* **24**, 4 (2022).
38. Payan, M., Khoshghalb, A., Senetakis, K. & Khalili, N. Effect of particle shape and validity of Gmax models for sand: A critical review and a new expression. *Comput. Geotech.* **72**, 28–41 (2016).
39. Khodkari, N., Hamidian, P., Khodkari, H., Payan, M. & Behnood, A. Predicting the small strain shear modulus of sands and sand-fines binary mixtures using machine learning algorithms. *Transp. Geotech.* **44**, 101172 (2024).
40. Clayton, C. R. I., Abbireddy, C. O. R. & Schiebel, R. A method of estimating the form of coarse particulates. *Géotechnique* **56**(6), 493–501 (2009).
41. Abbireddy, C. O. R. & Clayton, C. R. I. A review of modern particle sizing methods. *Proc. Inst. Civ. Eng. Geotech. Eng.* **162**(4), 193–201 (2009).
42. Karabash, Z. & Cabalar, A. F. Shear strength response of clay and sand column with different sand grain shapes. *Geomech. Eng.* **35**(2), 135–147 (2023).
43. Ministry of Water Resources of the People's Republic of China. *The Standard of China Specification of Soil Test (SL237-1999): Specification of Soil Test* (China Water Power Press, 1999).

Acknowledgements

We acknowledge the financial support by the Hubei Provincial Science and Technology Department Natural Science Foundation Youth Project (2023AFB339), the Hubei Provincial Education Department Science and Technology Research Program Young Talent Project(Q20222701), and the Natural Science Foundation of Xiaogan XGKJ2024030010. We also thank all the reviewers who participated in the review and MJ Editor (<https://www.mjeditor.com/>) for providing English editing services during the preparation of this manuscript.

Author contributions

Biwen Zhang and Xinlian Chen performed the building plan. Li Zhong and Yani Lu performed the specimen preparation and conducted the tests. Mingxing Luo, and Yan Wu conducted the discussions. Zhijiang Li, Biwen

Zhang and Li Zhong performed the data analysis and wrote the manuscript.

Declarations

Competing interests

The authors declare no competing interests.

Additional information

Correspondence and requests for materials should be addressed to B.Z., Y.L. or L.Z.

Reprints and permissions information is available at www.nature.com/reprints.

Publisher's note Springer Nature remains neutral with regard to jurisdictional claims in published maps and institutional affiliations.

Open Access This article is licensed under a Creative Commons Attribution-NonCommercial-NoDerivatives 4.0 International License, which permits any non-commercial use, sharing, distribution and reproduction in any medium or format, as long as you give appropriate credit to the original author(s) and the source, provide a link to the Creative Commons licence, and indicate if you modified the licensed material. You do not have permission under this licence to share adapted material derived from this article or parts of it. The images or other third party material in this article are included in the article's Creative Commons licence, unless indicated otherwise in a credit line to the material. If material is not included in the article's Creative Commons licence and your intended use is not permitted by statutory regulation or exceeds the permitted use, you will need to obtain permission directly from the copyright holder. To view a copy of this licence, visit <http://creativecommons.org/licenses/by-nc-nd/4.0/>.

© The Author(s) 2025